Thermal and chemical diffusion in the rapid solidification of binary alloys

Massimo Conti
Dipartimento di Matematica e Fisica, Universitá di Camerino, and Istituto Nazionale di Fisica della Materia, Via Madonna delle Carceri, I-62032, Camerino, Italy

(Received 28 June 1999; revised manuscript received 21 September 1999)

Solidification of binary alloys is characterized by the necessity to reject away from the advancing front two conserved quantities: the latent heat released at the solid-liquid interface and the solute atoms that cannot be accommodated in the solid phase. As thermal diffusion is much faster than chemical diffusion, the latter is generally assumed to be the rate limiting mechanism for the process, and the problem is addressed through the isothermal approximation. In the present paper we use the phase-field model to study the planar growth of a solid germ, nucleated in its undercooled melt. We focus on the effects of a noninstantaneous thermal relaxation. The steady growth predicted at large supersaturation in the isothermal limit is prevented. Depending on the value of the Lewis number the growth rate is limited by either mass or heat diffusion; in the latter case we observe a sharp transition between two different regimes, in which originates a nonmonotonic time dependence of the interface temperature. The effects of this transition reflect in the composition of the solidified alloy.

PACS number(s): 64.70.Dv, 68.10.Gw, 81.30.Bx, 82.65.Dp

I. INTRODUCTION

In rapid solidification processes the interfacial dynamics is the result of a competition between the nonequilibrium conditions imposed at infinity and the necessity to reject at least one conserved quantity away from the advancing front. For pure substances the growth is controlled by the diffusion of the latent heat released at the solid-liquid interface; for alloy solidification (the subject of the present study) both heat and solute diffusion are the limiting factors to the growth process.

The classical approach to describe the interfacial dynamics is formulated in terms of a moving boundary problem [1,2]. The diffusion equation is utilized to model the transport of heat and solute through the bulk phases. The interface boundary conditions reflect two different constraints: (i) the energy and solute conservation across the moving front, and (ii) constitutive laws that relate the local interface conditions (concentration c and temperature T) to the front velocity v. As the relaxation of the thermal field is much faster than the rearrangement of chemical species the process is often treated as isothermal. In this limit Langer [3] pointed out that, assuming local interfacial equilibrium and considering the chemical potential rather than the solute concentration as the diffusive field, the model for alloy solidification can be formally mapped onto the same set of governing equations which describe the solidification of a pure substance. The relevance of nonequilibrium effects in rapid solidification processes was pointed out by Aziz, Aziz, and Kaplan and Aziz and Boettinger [4–6]. Within the continuous growth model (CGM) they were able to explain the phenomenon termed ''solute trapping,'' that is the increase of the partition coefficient k (the ratio c_s/c_l of the solute concentration in the growing solid to that in the liquid at the interface) from the equilibrium value k_e towards unity at large growth rates.

A more recent approach to investigate alloy solidification is based on the phase-field model (PFM) [7–13]. In this model an order parameter characterizes the phase of the system at each point. A suitable free-energy functional is then constructed that depends on the order parameter as well as on the concentration and temperature fields and their gradients. The extremization of the functional in respect to these variables results in the dynamic equations for the process. Several theoretical and numerical studies [14–20] pointed out that the PFM describes in a natural fashion nonequilibrium effects as solute trapping and the kinetic undercooling of the solid-liquid interface.

Basing on these models, the growth process has been studied in different regimes, generally neglecting the dynamics of the thermal field. However, recent investigations pointed out that thermal diffusion enters as an essential ingredient into the evolution of the phase-change process. For example, the latent heat released at the interface significantly reduces the region of the parameters space where an oscillatory instability of the solidification front can be expected [21–23]. Moreover, in a previous study [24] the author showed that in the planar growth from a supercooled melt steady growth solutions, allowed within the isothermal approximation, are lost and the steady growth is driven into a diffusive regime. Then the effect of the heat diffusion on the solidification of binary alloys is an interesting and still open question.

In the present study this point will be addressed simulating the planar growth of a solid germ with the phase-field model. Extending the results of a previous work [24], we shall analyze the growth process at large supersaturation. It will be shown that, depending on the value of the Lewis number (i.e., the ratio of the chemical to the thermal diffusivity), the growth rate is limited by either mass or heat diffusion. At $\mathrm{Le}=0$ (i.e., with isothermal growth) after an initial transient steady growth is attained. With Le values characteristic of metallic alloys the process enters a diffusive regime governed by the rejection of solute at the interface, and the front velocity decays with time as $v \propto t^{-1/2}$. At inter-

mediate values of the thermal diffusivity an interesting phenomenon arises: the process undergoes a sharp transition between two different regimes. The first stage is characterized by a high growth rate which, however, decays with the power law $\propto t^{-1/2}$. In this stage the interface temperature increases with time, and the concentration field shows a strong trapping of solute into the solid phase. Then, when the interface temperature reaches a value near the T_0 line (where the Helmoltz free energies of the liquid and solid are equal), an abrupt transition turns the process into a low velocity regime, still characterized by the diffusive power law. The interface temperature is now decreasing with time, and the solute segregation at the interface approaches the equilibrium pattern.

The paper is organized as follows: in Sec. II the governing equations of the model will be derived, through the extremization of an entropy functional. In Sec. III the numerical method will be explained, and in Sec. IV the results of the numerical simulations will be discussed. The conclusions will follow in Sec. V.

II. THE GOVERNING EQUATIONS

The solidification of an ideal solution of components A (solvent) and B (solute) is described in terms of the scalar phase field ϕ, the local solute concentration c, and temperature T. The field ϕ is an order parameter assuming the values $\phi=0$ in the solid and $\phi=1$ in the liquid; intermediate values correspond to the interface between the two phases. The model directly follows the formulation given by Warren and Boettinger [25] and incorporates also many of the ideas developed by Caginalp and Xie [17], Caginalp and Jones [16], Wheeler *et al.* [14,15]. Full details of the derivation are presented elsewhere [26], and for the sake of conciseness we shall give below only a short review. As a starting point the entropy of the system is written as

$$\mathcal{S}=\int\left[s(e,\phi,c)-\frac{\epsilon^2}{2}|\nabla\phi|^2\right]dv, \tag{1}$$

where integration is performed over the system volume; the last term in the integrand is a gradient correction to the thermodynamic entropy density s, that depends on the internal energy density e, and on the concentration and phase fields. To ensure a positive local entropy production, the governing equations for the phase and solute fields can be written as

$$\dot{\phi}=M_\phi\frac{\delta\mathcal{S}}{\delta\phi}, \tag{2}$$

$$\dot{c}=-\nabla\cdot\left(M_c\nabla\frac{\delta\mathcal{S}}{\delta c}\right), \tag{3}$$

and for the energy density,

$$\dot{e}=-\nabla\cdot\left(M_e\nabla\frac{\delta\mathcal{S}}{\delta e}\right), \tag{4}$$

where M_c, M_ϕ and M_e are positive constants. Assuming a double-well Ginzburg-Landau free energy for the pure constituents, and evaluating the functional derivatives, gives

$$\frac{\partial\phi}{\partial t}=M_\phi[\epsilon^2\nabla^2\phi-(1-c)\tilde{H}^A(\phi,T)-c\tilde{H}^B(\phi,T)], \tag{5}$$

$$\frac{\partial c}{\partial t}=-\nabla\cdot\left\{D_c c(1-c)\frac{v_m}{R}[\tilde{H}^A(\phi,T)-\tilde{H}^B(\phi,T)]\nabla\phi - D_c\nabla c+D_c c(1-c)\frac{v_m}{R}\tilde{\Gamma}(\phi,T)\nabla T\right\}, \tag{6}$$

$$\frac{\partial T}{\partial t}=D_T\nabla^2 T-\frac{1}{\chi}[(1-c)L^A+cL^B] \times\frac{dp(\phi)}{d\phi}\frac{\partial\phi}{\partial t}-\frac{1}{\chi}p(\phi)(L^B-L^A)\frac{\partial c}{\partial t}. \tag{7}$$

In Eqs. (5)–(7) R is the gas constant and v_m is the molar volume; the solute diffusivity is defined as $D_c=(M_c R)/[v_m c(1-c)]$ and the thermal diffusivity as $D_T=M_e/(\chi T^2)$, being χ the specific heat, for which we assume equal values for both components in both phases. The function $\tilde{H}^A(\phi,T)$ is defined as

$$\tilde{H}^A(\phi,T)=\frac{dG^A(\phi)}{d\phi}-\frac{dp(\phi)}{d\phi}L^A\frac{T-T^A}{TT^A}, \tag{8}$$

where

$$G^A(\phi)=\frac{1}{4}\tilde{W}^A\phi^2(1-\phi)^2=\tilde{W}^A g(\phi) \tag{9}$$

is a symmetric double-well potential with equal minima at $\phi=0$ and $\phi=1$, scaled by the positive well height $\tilde{W}^A$; L^A and T^A are the latent heat per unit volume and the melting temperature of the pure component pure A; choosing the function $p(\phi)$ as $p(\phi)=\phi^3(10-15\phi+6\phi^2)$ the condition is enforced that bulk solid and liquid are described by $\phi=0$ and $\phi=1$, respectively, for every value of temperature [12].

Equations (8) and (9) still hold for $\tilde{H}^B(\phi,T)$ and $G^B(\phi)$ if all the material parameters, labeled with the superscript A are replaced with the ones related to the B species. The function $\tilde{\Gamma}(\phi,T)$ is defined as

$$\tilde{\Gamma}(\phi,T)=-\frac{p(\phi)}{T^2}(L^A-L^B). \tag{10}$$

To allow for different diffusivities in the solid and liquid phases, in the following D_c will be taken as $D_c=D_s+p(\phi)(D_l-D_s)$, D_l and D_s being the diffusivities in the liquid and in the solid, respectively.

Equations (5)–(7) will be rephrased scaling lengths to some reference length ξ and time to ξ^2/D_l. Allowing M_ϕ to depend on the local composition as $M_\phi=(1-c)M_\phi^A+cM_\phi^B$, and following the lines suggested by Warren and Boettinger [25] to associate the model parameters to the material properties, the governing equations become

$$\frac{\partial \phi}{\partial t}=[(1-c)m^A+c\,m^B]\times[\nabla^2\phi+(1-c)Q^A(T,\phi)+cQ^B(T,\phi)], \quad (11)$$

$$\frac{\partial c}{\partial t}=-\nabla\cdot\{c(1-c)\lambda(\phi)[H^A(\phi,T)-H^B(\phi,T)]\nabla\phi + c(1-c)\lambda(\phi)\Gamma(\phi,T)\nabla T-\lambda(\phi)\nabla c\}, \quad (12)$$

$$\frac{\partial T}{\partial t}=\frac{1}{\mathrm{Le}}\nabla^2 T-\frac{1}{\chi}[(1-c)L^A+cL^B]\times\frac{dp(\phi)}{d\phi}\frac{\partial\phi}{\partial t}-\frac{1}{\chi}p(\phi)(L^B-L^A)\frac{\partial c}{\partial t}, \quad (13)$$

where Le is the Lewis number, defined as $\mathrm{Le}=D_c/D_T$, and

$$H^{A,B}(\phi,T)=W^{A,B}\frac{dg(\phi)}{d\phi}-L^{A,B}\frac{v_m}{R}\frac{dp(\phi)}{d\phi}\frac{T-T^{A,B}}{TT^{A,B}} = \frac{v_m}{R}\tilde{H}^{A,B}(\phi,T), \quad (14)$$

$$Q^{A,B}(\phi,T)=-\frac{\xi^2}{(h^{A,B})^2}\frac{dg(\phi)}{d\phi}+\frac{1}{6\sqrt{2}}\frac{\xi^2 L^{A,B}}{\sigma^{A,B}h^{A,B}}\frac{T-T^{A,B}}{T_\infty}\frac{dp(\phi)}{d\phi}, \quad (15)$$

$$\Gamma(\phi,T)=\frac{v_m}{R}\tilde{\Gamma}(\phi,T), \quad (16)$$

$$\lambda(\phi)=\frac{D_s}{D_l}+p(\phi)\left(1-\frac{D_s}{D_l}\right). \quad (17)$$

In Eq. (15) $\sigma^{A,B}$, $h^{A,B}$ indicate the surface tension and the interface thickness of the pure components A and B, respectively; T_∞ is the initial melt temperature. The model parameters $m^{A,B}$, $W^{A,B}$ depend on the physical properties of the alloy components through

$$m^{A,B}=\frac{\beta^{A,B}\sigma^{A,B}T^{A,B}}{D_l L^{A,B}}, \quad W^{A,B}=\frac{12}{\sqrt{2}}\frac{v_m}{R}\frac{\sigma^{A,B}}{T^{A,B}h^{A,B}}, \quad (18)$$

where $\beta^{A,B}$ is the kinetic undercooling coefficient of pure A or B, that relates the interface temperature T_I to the interface velocity v through $v=\beta^{A,B}(T^{A,B}-T_I)$.

To conduct the numerical simulations we referred to the phase diagram of an ideal solution of nickel (solvent) and copper (solute), using the data summarized in Table I; the solute diffusivity in the solid phase was estimated as $D_s=10^{-6}\times D_l$. The length scale was fixed at $\xi=2.1\times10^{-4}$cm; the kinetic undercooling coefficients were fixed to $\beta^A=128.64\ \mathrm{cm\,s^{-1}K^{-1}}$ and $\beta^B=153.60\ \mathrm{cm\ s^{-1}K^{-1}}$, not far from the actual best estimates [29] and a realistic value for the interface thickness was selected as 1.68×10^{-7} cm. Using the above values it results that $W^A=0.963$; $W^B=0.960$; $m^A=m^B=350$.

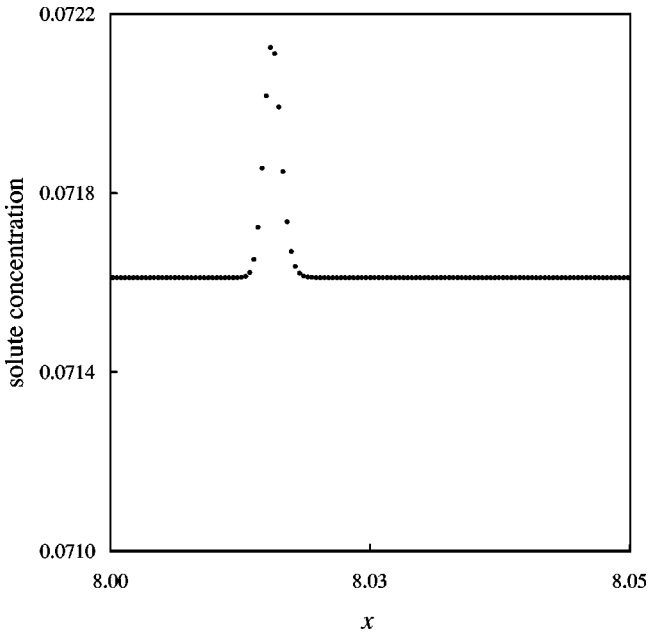

FIG. 1. The concentration profile for Le=0 (i.e., isothermal growth), at time $t=10^{-3}$.

III. THE NUMERICAL METHOD

The evolution of Eqs. (11)–(13) has been considered in one spatial dimension, with fluxless boundary conditions $\phi_x=c_x=T_x=0$ at the domain's walls. Initially in the undercooled melt, at uniform temperature and concentration T_∞ and c_∞, a solid germ was nucleated in the region $0\leqslant x\leqslant x_0$ with a composition equal to c_∞. To discretize the equations second order in space and first order in time finite-difference approximations were utilized. Then, an explicit scheme was employed to advance forward in time the phase field and concentration equations; the temperature equation was more conveniently integrated with a fully implicit method. The choice of the computational grid posed some delicate problems. The physical process involves intrinsic and quite different length scales. The width of the phase field and concentration transition layer, across the interface, is of the order of 10^{-3} (nondimensional units); the solute diffusion length, in our simulations, was in the range 10^{-2}–10^0, while the thermal diffusion length reached values as high as 10^4. The necessity to avoid finite-size effects and, at the same time, to resolve accurately the phase and concentration fields, suggested the division of the computational domain into two parts: an inner region, of interest for the phase and concen-

TABLE I. Material parameters for the Ni-Cu alloy.

Parameter	Nickel	Copper
T_m (K)	1728	1358
L (J/cm^3)	2350	1728
v_m (cm^3/mole) [a]	7.0	7.8
σ (J/cm^2)	3.7×10^{-5}	2.8×10^{-5}
β (cm/K s) [b]	128.64	153.60
D_l (cm^2/s)	10^{-5}	10^{-5}

[a]An average value of 7.4 will be taken.
[b]From the estimation of Willnecker *et al.* [29].

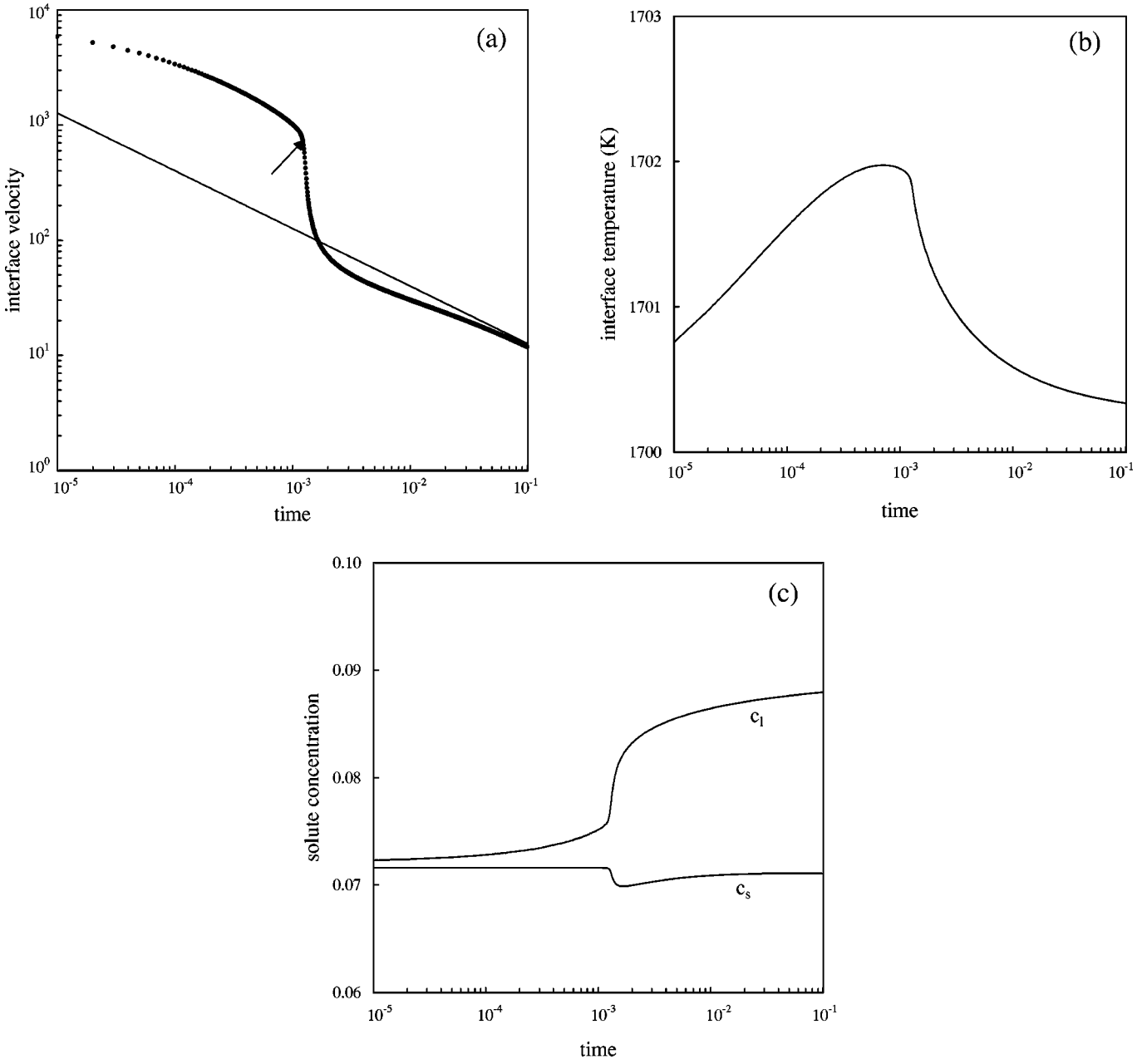

FIG. 2. The interface velocity (a), the interface temperature (b), and the solute concentration at the interface (c) versus time. Le$=6.45\times10^{-9}$. The straight line in (a) is representative of the power law $\propto t^{-1/2}$, and the arrow indicates the operating point corresponding to the maximum acceleration.

tration dynamics, and an outer region, where only the temperature equation was integrated. In the inner region $0\leqslant x\leqslant x_i$ the grid spacing was selected as $\Delta x_i=4\times10^{-4}$, that is half of the nominal interface thickness. This value was a standard choice in previous studies [18,19,24], where it was proven to ensure accurate solutions of the phase and concentration equations. In the outer region $x_i\leqslant x\leqslant x_o$, we used a nonuniform grid, stretching the mesh spacing with the law $\Delta x_o=\Delta x_i+\Delta x_\infty[1-\exp((x-x_i)/x_L)]$. The values of Δx_∞ and x_L were chosen, for each simulation, to ensure accuracy as well as computational economy; in any case the temperature field was never resolved with less than 4×10^4 grid points, and the temperature differences between adjacent grid points never exceeded 10^{-3} K.

For the same reason of computational economy, even along the time axis we used different grids. The concentration equation (12) requires, for numerical stability, a time step Δt_c which scales as $(\Delta x)^2/D_l$, being $D_l=1$. On the other side, the phase-field equation (11) is a diffusion-reaction equation with diffusivity $D_\phi=m^{A,B}=350$; in this case the time step for stability Δt_ϕ is expected to scale as $(\Delta x)^2/D_\phi$. No stability problems arise for the temperature equation, which is integrated with an implicit method with a time step $\Delta t_T=\Delta t_c$. Due to the large value of D_ϕ, we used a value for Δt_ϕ much smaller than $\Delta t_T=\Delta t_c$. In practice we iterated 320 times the phase-field equation within a single time step (equal to 5×10^{-8}) of the temperature and concentration equations.

The convergence of the numerical scheme was checked accurately in different cases with respect to the refinement of

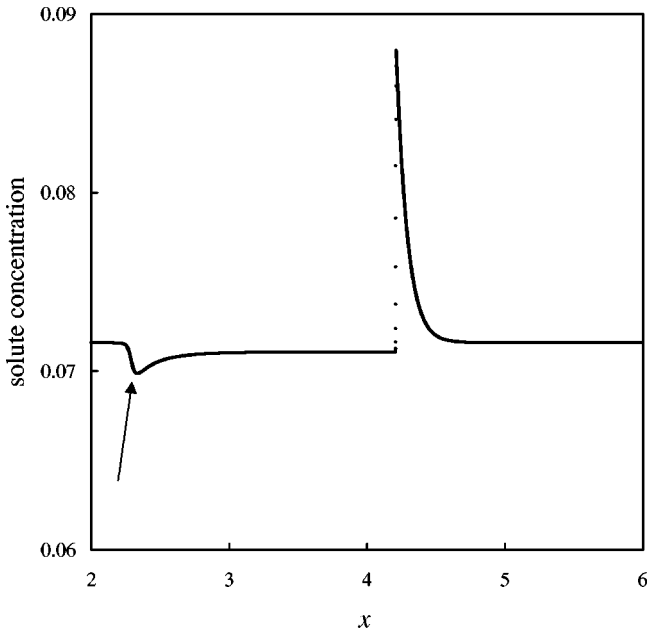

FIG. 3. The concentration profile with $\mathrm{Le}=6.45\times10^{-9}$, at time $t=10^{-1}$. The arrow indicates the effect of the sharp decrease of the growth rate.

the computational grid in both the outer and the inner region; moreover we checked that using a different time step for the phase-field equation had no influence on the numerical results.

IV. NUMERICAL RESULTS

The isothermal version of the model, corresponding to $\mathrm{Le}=0$ was analyzed in a previous study [18]; for the reader's commodity we assume here some of the main results. We fixed $T_\infty=1700$ K corresponding to equilibrium concentrations, on the solidus and liquidus lines, respectively, $c_s^*=0.071\,611$ and $c_l^*=0.089\,945$; the concentration of the melt was set to $c_\infty=c_s$, on the solidus line. With these values after a short transient the process reaches a steady state and the solid-liquid front advances at constant velocity $v=7973$. Here and in the following, except for temperature, physical quantities will be expressed in nondimensional units. In Fig. 1 we show the solute profile taken at $t=10^{-3}$. The peak of the curve, $c_l=7.2129\times10^{-2}$ identifies the liquid side of the interface; the dynamic partition coefficient is $k(v)=c_\infty/c_l=0.992\,81$. To compare these results

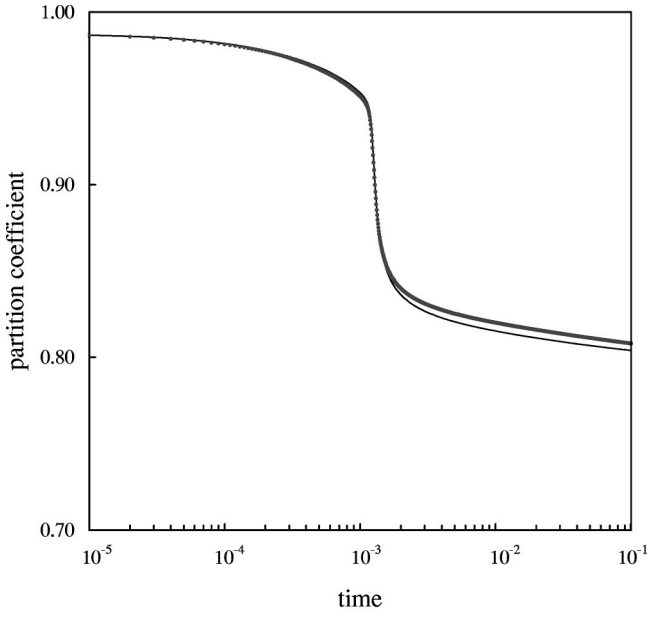

FIG. 4. The actual partition coefficient (solid circles) compared with the predictions of Eq. (19) (solid line) during the growth process. The agreement between the two sets of data is within 0.5%.

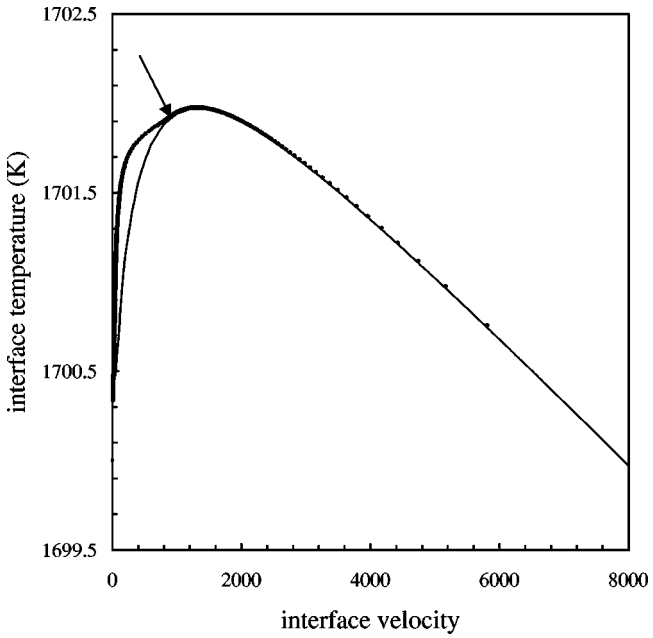

FIG. 5. The interface temperature versus the interface velocity. The solid line refers to the steady solutions for isothermal growth. The solid circles refer to the present numerical solution, with $\mathrm{Le}=6.45\times10^{-9}$. The arrow indicates the effect of the sharp decrease of the growth rate.

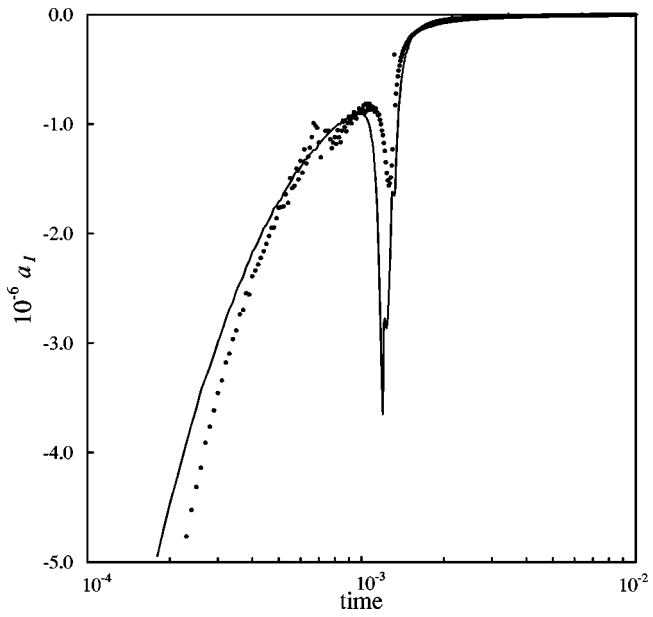

FIG. 6. The actual interface acceleration (solid line), compared with the predictions of Eq. (21).

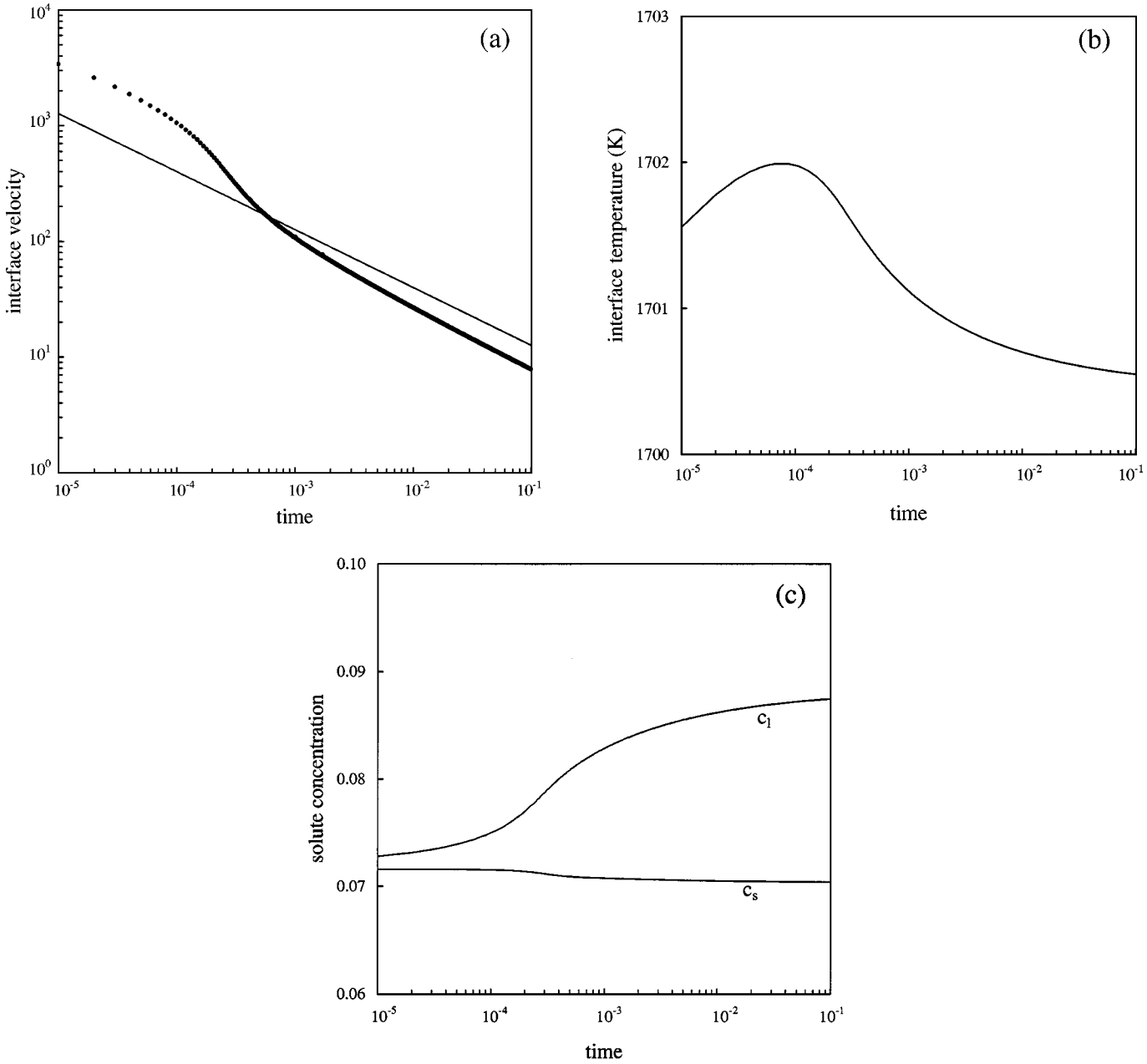

FIG. 7. The interface velocity (a), the interface temperature (b), and the solute concentration at the interface (c) versus time. Le$=6.45\times10^{-8}$. The straight line in (a) is representative of the power law $\propto t^{-1/2}$.

with the predictions of the continuous growth model (CGM) we recall that the latter gives, for steady growth, the dependence of the partition coefficient and the interface temperature on the growth velocity in the form:

$$k(v)=\frac{k_e+v/v_d}{1+v/v_d}, \tag{19}$$

$$T_I(v)=T^A+\frac{m_l c_l}{1-k_e}\{1-k+[k+(1-k)\gamma]\ln(k/k_e)\}-\frac{v}{\beta^A}, \tag{20}$$

k_e being the equilibrium value for a stationary interface ($k_e=0.797$ in our case), and v_d is the diffusional velocity for the solute redistribution across the moving front; v_d is generally expressed as $v_d=D/a$, where D is an interface diffusivity and a is the width of the concentration transition layer. The slope of the equilibrium liquidus line is indicated as m_l and the parameter γ describes the dissipation of free energy due to solute drag across the interface: this phenomenon is completely neglected with $\gamma=0$ and accounted for with $\gamma=1$.

A previous investigation [19] identified a best value of $v_d=290$ and $\gamma=0.65$; with these values Eqs. (19), (20) give $k(v)=0.992\,84$ and $T_I(v)=1700.04$ K, respectively, which is in good agreement with the numerical data.

A quite different picture emerges when the dynamics of the thermal field is taken into account, assuming a high but finite thermal diffusivity. We set $D_T=15.5\times10^7$, that is larger than the actual values characteristic of metallic alloys by a factor of 10^4; this means Le$=6.45\times10^{-9}$. Figure 2(a) shows the interface velocity versus time (circles). The solid line is representative of the diffusive law $\propto t^{-1/2}$. In a first

stage the process is characterized by a high growth rate; the interface slows down with a slope not far from $-1/2$. At $t=10^{-3}$ we observe a transition; the interface velocity is suddenly decreased of an order of magnitude and finally reaches a new diffusive regime. The sharp transition from the high velocity to the low velocity regime is reflected on the time dependence of the interface temperature T_I, shown in Fig. 2(b). During the first stage T_I increases, reaching a maximum of 1701.97 K. Then, in the low velocity regime T_I decreases with time. Figure 2(c) shows versus time c_s and c_l, i.e., the solute concentration on the solid side and the liquid side of the interface, respectively. As expected at high velocities, due to solute trapping, the concentration gap at the interface is very low (and increasing with time). Subsequent to the abrupt decrease of the growth rate we observe that the solute redistribution across the interface becomes more effective and the gap suddenly increases. The sharp transient leaves a trace in the solidified alloy. In Fig. 3 we see the solute profile at $t=10^{-1}$: the negative peak indicated by the arrow reflects the depletion of solute on the solid side of the interface shown in Fig. 2(c).

A clear theoretical explanation for the phenomena described in the above pictures is at present difficult to find, as they originate from the complex interplay between the rejection of both heat and solute away from the advancing front. However, to get some insight into this interesting behavior we can start from an analysis of the two diffusional time scales. Being that $D_c/v^2 \ll D_T/v^2$, we expect a quasi-instantaneous adaptation of the solute field to the variations of the thermal field. Moreover, Eqs. (19) and (20), derived for steady growth, are generally assumed to work even for time-dependent processes when the time variation of the interface temperature is sufficiently slow in respect to the characteristic time for the solute relaxation across the interface, that is $\tau \sim a^2/D = a/v_d$. In the present case we have $\tau < 10^{-5}$ and this condition is likely to be fulfilled except, perhaps, immediately after the transition [see Fig. 2(b)] where we observe a high rate of change of $T_I(t)$. Then, if the interfacial temperature is consistent with a steady solution for isothermal growth it seems reasonable to decouple to some extent the heat and solute diffusion, assuming that the phase and solute fields evolve with a quasisteady dynamics, following the local (interfacial) temperature conditions. This suggestion is confirmed observing in Fig. 4, along the entire process, the close agreement (within 0.5%) between the values of the actual partition coefficient and the predictions of Eq. (19).

On the other side, Eq. (20), as well as analytical and numerical studies based on the phase-field model, were able to fix, for a given supersaturation, the conditions for isothermal steady growth. The interface temperature is a nonmonotonic function of the interface velocity, resulting from the competition of two opposite effects. At low velocities, due to solute trapping (and to the consequent reduction of solute concentration on the liquid side of the interface), T_I is an increasing function of v. At higher velocities the undercooling required to advance the solidification front becomes important: the $T_I(v)$ curve traverses a maximum near the T_0 line (where the Helmoltz free energies of the liquid and solid are equal; $T_0 = 1703.01$ K in our case) and then exhibits a descending branch. In the low velocity branch of the curve the driving force for the process (i.e., the thermodynamic undercooling) is a decreasing function of the associate flux (the growth rate), resulting in unstable growth. Notice that for temperatures above the maximum of the $T_I(v)$ curve the growth process is characterized by a diffusive regime, with the rate limiting mechanism due to chemical diffusion. Figure 5 shows, in the v,T plane the locus of steady solutions for isothermal growth (solid line). These data, quoted from a previous study, have been obtained solving the model in directional solidification conditions and fit, in quite good agreement, the predictions of Eq. (20) [19]. On the same graph we superimposed (solid circles) the path described by the operating point of the process. We see that during the high velocity regime the process evolves strictly along the stable branch of the steady $T_I(v)$ curve, indicating that the quasisteady assumption is well satisfied. As expected, we observe a deviation between the two sets of data across the transition and immediately after, when the process is driven towards the low velocity branch of the curve. The above considerations show that the interface dynamics is substantially slaved by the evolution of the thermal field, and the rejection of heat is the limiting mechanism for the process.

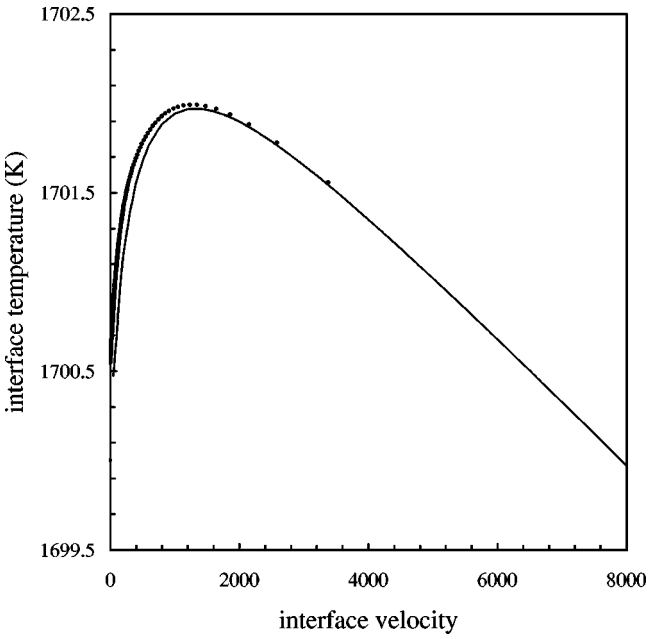

FIG. 8. The interface temperature versus the interface velocity. The solid line refers to the steady solutions for isothermal growth. The solid circles refer to the present numerical solution, with Le $=6.45\times10^{-8}$.

The sudden jump of the interface velocity shown in Fig. 2(a) can be explained writing an equation for the acceleration of the solid-liquid front in the form:

$$a_I = \frac{dv}{dT_I} \cdot \frac{dT_I}{dt}. \tag{21}$$

We see that near the maximum of the $T_I(v)$ curve the front acceleration given by Eq. (21) is infinite, as $dT_I/dv = 0$ and the transition between the high and low velocity regimes is described as instantaneous [in this limit, obviously, the quasisteady approximation is no longer valid and Eq. (21) fails to work]. The arrows drawn in Figs. 2(a) and 5 indicate the operating point corresponding to the maximum

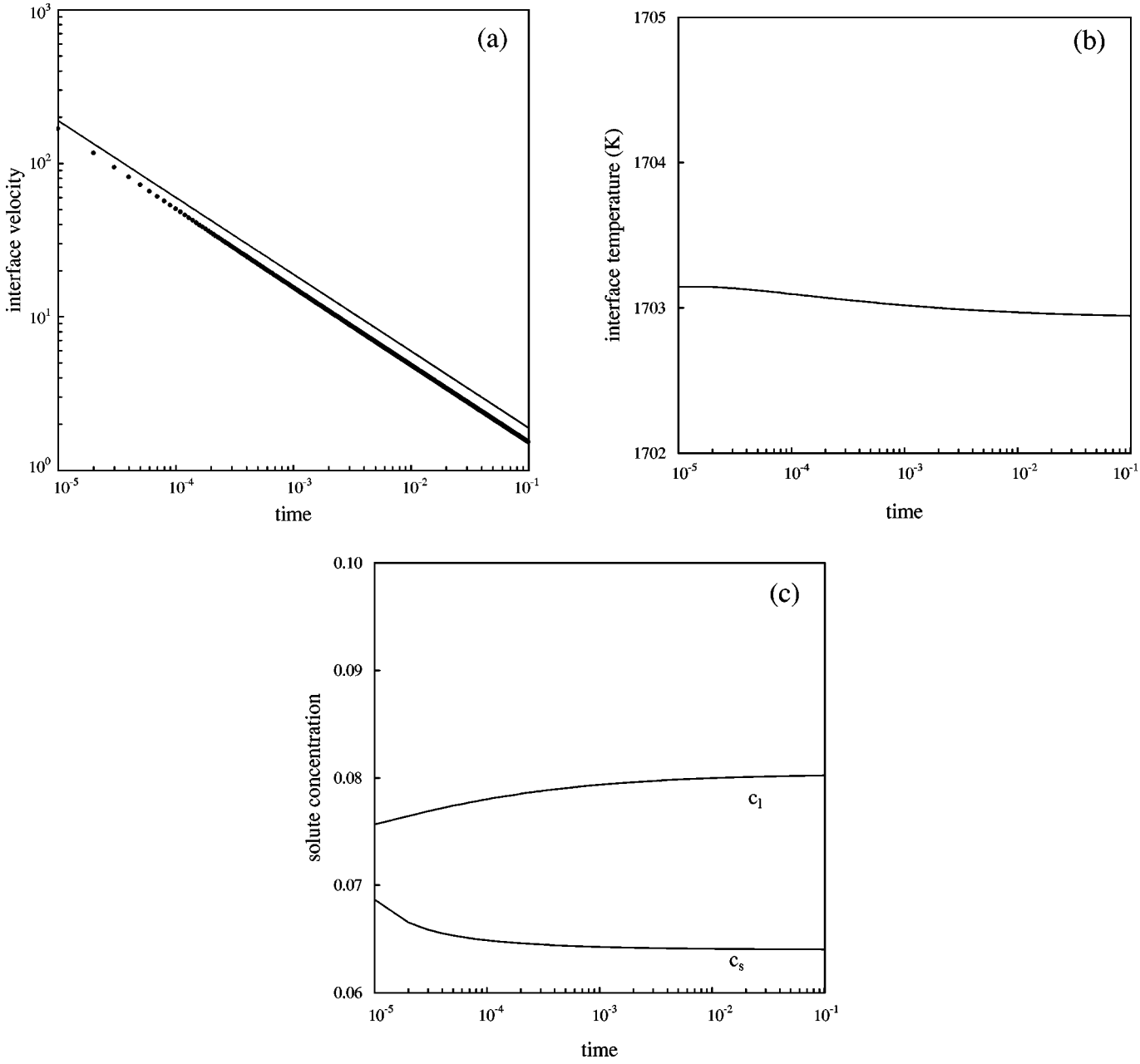

FIG. 9. The interface velocity (a), the interface temperature (b), and the solute concentration at the interface (c) versus time. Le$=6.45\times10^{-5}$. The straight line in (a) is representative of the power law $\propto t^{-1/2}$.

interface acceleration ($t=1.19\times10^{-3}, v=823$), which is indeed very close to the maximum of $T_I(v)$. To better clarify this issue, Fig. 6 shows the interface acceleration, as given by Eq. (21) (solid circles) compared with the results of our simulation (solid line). The dependence $T_I(t)$ in Eq. (21) is extracted from the numerical data. We see that the main features of the actual interface acceleration are captured by the above simple picture to a good extent of accuracy. It is worth noting that sharp transitions between the stable and unstable branches of the $T_I(v)$ curve were observed also in the dynamics of the banding phenomena [21,27,28] and were ascribed to the same mechanism.

In Figs. 7(a)–7(c) we show the data obtained with Le $=6.45\times10^{-8}$. We still observe a transition of the process between a high and a low velocity regime but the transition is here much slower than in the previous case and the quasisteady picture should work much better. This is confirmed in Fig. 8 where we see that the actual interface dynamics closely follows the steady $T_I(v)$ dependence.

When the Lewis number is further increased the rejection of heat becomes less effective and the interface warms up. Eventually the interface temperature reaches values above the steady $T_I(v)$; then the quasisteady picture breaks down, and the growth process enters a diffusive regime governed by the rejection of solute. This situation is illustrated in Figs. 9(a)–9(c) obtained with a Lewis number Le$=6.45\times10^{-5}$ characteristic of metallic alloys. We see that along the entire duration of the process the interface velocity follows the diffusive law $\propto t^{-1/2}$ and the interface temperature is close to 1703 K, well above the limit for isothermal steady growth. The concentration gap at the interface c_l-c_s increases with time, approaching asymptotically the equilibrium value.

V. CONCLUSIONS

Rapid solidification of binary alloys is generally addressed in the isothermal approximation, because of the large ratio of heat to solute diffusivity. On the contrary, the results of the present study show that the evolution of the thermal field is of central interest to understand the interface dynamics. The steady growth regime, predicted at large supersaturation when Le=0, is no longer allowed when thermal diffusion is taken into account. The different time scales characteristic of thermal and chemical diffusion allow one to decouple to some extent the two processes. At low values of the Lewis number the growth rate is determined by the steady solutions consistent with the interface temperature; a transition between high and low velocity states is observed, accordingly to the nonmonotonic dependence $T_I(v)$. This simple picture allows one to predict the interface acceleration with some accuracy. The effects of the transition can be observed through the solute field frozen in the solidified alloy. As the Lewis number increases, the interface warms up, and the process enters a regime in which the rate limiting mechanism is the diffusion of solute.

[1] D. A. Kessler, J. Koplik, and H. Levine, Adv. Phys. **37**, 225 (1988).
[2] M. C. Flemings, *Solidification Processing* (McGraw-Hill, New York, 1974).
[3] J. S. Langer, Rev. Mod. Phys. **52**, 1 (1980).
[4] M. J. Aziz, J. Appl. Phys. **53**, 1158 (1982).
[5] M. J. Aziz and T. Kaplan, Acta Metall. **36**, 2335 (1988).
[6] M. J. Aziz and W. J. Boettinger, Acta Metall. Mater. **42**, 527 (1994).
[7] G. Caginalp, in *Applications of Field Theory to Statistical Mechanics*, Vol. 216 of *Lectures Notes in Physics*, edited by L. Garrido (Springer, Berlin, 1984), p. 216.
[8] G. Caginalp, Arch. Ration. Mech. Anal. **92**, 205 (1986).
[9] G. Caginalp and P. Fife, Phys. Rev. B **33**, 7792 (1986).
[10] G. Caginalp, Phys. Rev. A **39**, 5887 (1989).
[11] O. Penrose and P. C. Fife, Physica D **43**, 44 (1990).
[12] S. L. Wang, R. F. Sekerka, A. A. Wheeler, B. T. Murray, S. R. Coriell, R. J. Braun, and G. B. McFadden, Physica D **69**, 189 (1993).
[13] Zhiqiang Bi and Robert F. Sekerka, Physica A **261**, 95 (1998).
[14] A. A. Wheeler, W. J. Boettinger, and G. B. McFadden, Phys. Rev. A **45**, 7424 (1992).
[15] A. A. Wheeler, W. J. Boettinger, and G. B. McFadden, Phys. Rev. E **47**, 1893 (1993).
[16] G. Caginalp and J. Jones, Ann. Phys. (N.Y.) **237**, 66 (1995).
[17] G. Caginalp and W. Xie, Phys. Rev. E **48**, 1897 (1993).
[18] M. Conti, Phys. Rev. E **55**, 701 (1997).
[19] M. Conti, Phys. Rev. E **56**, 3717 (1997).
[20] N. A. Ahmad, A. A. Wheeler, W. J. Boettinger, and G. B. McFadden, Phys. Rev. E **58**, 3436 (1998).
[21] A. Karma and A. Sarkissian, Phys. Rev. Lett. **27**, 2616 (1992).
[22] A. Karma and A. Sarkissian, Phys. Rev. E **47**, 513 (1993).
[23] M. Conti, Phys. Rev. E **58**, 6101 (1998).
[24] M. Conti, Phys. Rev. E **55**, 765 (1997).
[25] J. A. Warren and W. J. Boettinger, Acta Metall. Mater. **43**, 689 (1995).
[26] M. Conti, Phys. Rev. E **58**, 6166 (1998).
[27] M. Carrard, M. Gremaud, M. Zimmermann, and W. Kurz, Acta Metall. Mater. **40**, 983 (1992).
[28] M. Conti, Phys. Rev. E **58**, 2071 (1998).
[29] R. Willnecker, D. M. Herlach, and B. Feuerbacher, Phys. Rev. Lett. **62**, 2707 (1989).